Fuel 310 (2022) 122208

Contents lists available at ScienceDirect

Fuel

journal homepage: www.elsevier.com/locate/fuel

Full length article

A phenomenological model for near-nozzle fluid processes: Identification and qualitative characterisations

Dan Sykes [a], Viacheslav Stetsyuk [a], Jack Turner [a], Guillaume de Sercey [a], Martin Gold [b], Richard Pearson [b], Cyril Crua [a,*]

[a] Advanced Engineering Centre, University of Brighton, Brighton, UK
[b] BP Technology Centre, Pangbourne, UK

ARTICLE INFO

Keywords:
High-speed microscopy
Dribble
Split injections
Cavitation
Rarefaction
Fuel discharge
Gas ingestion
Surface films
Low load
Idling
Near-nozzle region
Injector deposits
Spray wetting

ABSTRACT

It is well established that emissions and inefficiencies primarily arise from localised fuel rich regions, which do not undergo complete combustion. In order to achieve significant reductions in NOx and soot, modern engines employ multiple injection and flow rate profiling strategies. However, during the end of each injection event, the needle restricts the internal flow of fuel, rapidly reducing the inertia of the emerging spray. Atomisation is inhibited and large fluid structures are released into the cylinder. Once the flow subsides, fuel films remain on the nozzle surface well into the cycle. Fuel residing in the nozzle cavities emerges as the cycles progresses, amalgamating with the spray deposited films. The surface-bound fuel presents an ideal environment for deposit forming reactions and a medium for precursors to adhere onto. In order to better understand these processes we performed measurements of injection transients inside an optical reciprocating rapid compression machine, using high-speed long-distance microscopy to obtain detailed characterisations of fuel films on the surface of an injector. We summarise our observations into a new phenomenological model which describes the uncontrolled release of fuel over an entire engine cycle. This model identifies the micro-scale processes that lead to the ejection, accumulation and vaporisation of fuel in-between injection events. Characterisation of these critical, transient processes can support mitigation strategies that inhibit pollutants and the formation of injector deposits.

1. Introduction

It is well established that the efficiency of an engine, as well as the exhaust gas composition, is primarily governed by the in-cylinder combustion of the fuel and thus, the preceding air-fuel mixing processes [1]. The properties of the fuel spray (i.e. the shape of the jet, the entrainment of hot gasses and behaviour of the individual liquid structures), dictate the characteristics of the vapour region encompassing the liquid jet and consequently, the combustion performance [2,3]. Autoignition occurs at several sites within the vapour phase then spreads throughout the vapour region [2], promoting evaporation of neighbouring fuel. The vaporised fuel is broken down releasing thermal energy whilst governing the production of soot [3,4]. Recent modifications to the in-cylinder components, in particular the fuel injection equipment, have led to enhanced control over the flow rate profile [5] and a refined spray atomisation (smaller, more dispersed droplets), thereby improving power delivery with a cleaner combustion. The modifications result in increased In-Cylinder Temperatures (ICT), gas pressures (ICP) and Injection Pressures (IP) (with commercial common rail system reaching pressures of over 300 MPa [6]). Despite the clear benefits of these modifications, the altered conditions in the immediate vicinity of the injector nozzle are thought to accelerate the formation of detrimental injector deposits [7–9]. Further design evolution including gradual reductions to nozzle geometries (i.e. increased number of smaller orifices, smaller sac sizes and reduced actuator control chambers), then increase the susceptibility of the nozzle to the detrimental effects of the deposits [10].

Internal diesel injector deposits and in-orifice fouling alter the precisely designed internal geometry of the nozzle thereby diverting the internal flow and cavitation behaviour from the ideal flow-field, compromising the subsequent atomisation [11]. External deposits and in-orifice fouling is primarily caused by coking, resulting from the thermal degradation of nozzle adhering fuel. In-orifice fouling reduces the flow rate and may effect the turbulent behaviour in the emerging jet [9,12]. Needle deposits cause potential misfire and even injector

* Corresponding author.
E-mail address: c.crua@brighton.ac.uk (C. Crua).
URL: http://www.brighton.ac.uk/staff/crua (C. Crua).

https://doi.org/10.1016/j.fuel.2021.122208
Received 16 June 2021; Received in revised form 17 September 2021; Accepted 3 October 2021

Nomenclature

Abbreviations

aTDC	After Top Dead Centre
bTDC	Before Top Dead Centre
CA	Crank Angle
EOI	End Of Injection
FWHM	Full Width Half Maximum
ICP	In-Cylinder Pressure
ICT	In-Cylinder Temperature
IP	Injection Pressure
SOI	Start Of Injection
TDC	Top Dead Centre
UHC	Unburnt Hydrocarbon
VCO	Valve Covered Orifice

failure due to seizure or sticking to the valve seat [13,14]. External nozzle surface deposits are the most commonly reported deposit type. However, they have been shown to have very little influence on the performance of diesel atomisation since the high IPs blast away any material protruding into the jet [15]. The lower IPs used in gasoline injectors mean that external coking poses a much larger problem, changing the spray shape and reducing fuel flow rate [16]. Although these deposit types typically occur in unison, a direct link between the mechanisms of each has not yet been established. In fact little is known about both the formation and growth mechanisms of all deposit types. That which is known is not entirely agreed upon [17], partly due to the great diversity of the cases studied. Nevertheless, it is known that there are important interactions between the nozzle surfaces/injector deposit, nozzle-residing fuel and the surrounding environment (the quenching gas layer encapsulating it in the case of coking), contributing towards deposit formation and diminishing engine durability [17–19].

Recent efforts directed towards optimisation of the spray plume have led to the use of fast-response piezo-actuated injectors, capable of forces greater than 800 N (8 times that of a solenoid injector generating less than 100 N [20]). The resulting improvements in dynamic response times reduce the period spent in the transient injection phases (i.e. needle valve opening and needle valve closing) and can give superior fuel-air mixing when compared to solenoid-actuated injectors [21,22]. These differences have been demonstrated to deter deposits while decreasing emissions [23]. Multiple injection and rate profiling strategies are also being implemented, increasing control over the injection rate to reduce unwanted combustion by-products and improving combustion efficiency. Pilot injections are used to smooth the ICP rise from combustion, while post injections are used to burn off Unburnt Hydrocarbons (UHC) and soot from the main combustion event [24,25]. There are however, diminishing returns, suggestive of a persistent source of pollutant emissions [26].

Increased use of split injection/rate profiling strategies place a greater proportion of the spray events within the transient spray regime (during needle ascent and descent when the internal flow is throttled), inhibiting the intended internal flow pattern. It is already known that the early and late phases of the injection produce large, slow, deformed and often surface-bound liquid structures [27,28]. It is likely that these structures are too large to undergo complete combustion, either producing detrimental combustion by-products or getting drawn into the exhaust where they directly contribute towards engine-out UHC emissions (pre after-treatment). Fuel films residing within the nozzle or on its outer surface have a strong potential for involvement in deposit formation through creation, absorption and catalyzation of precursors [17].

The nozzle residing fuel and near-nozzle conditions are almost entirely dependent of the transient injection regimes, and, as shown by this study, numerous other fluid phenomena occur within the post-injection phase. Several other researchers have looked at characterising both End Of Injection (EOI) and subsequent post-injection processes using experimental and numerical methods [19,29,30]. Moon et al. [31] conducted high-speed X-ray phase contrast imaging to gain insights into the internal and near-nozzle flow dynamics for a single hole diesel injector during needle valve closure. The high energy photons used in this technique are able to penetrate the injector tip and reveal details on internal processes through tracking of the phase boundaries. Vapour formation, air ingestion and EOI mass expulsion were all directly observed obtaining valuable information that not only allows the connection of internal and external phenomena, but also gives validation to several numerical studies in the literature [32–35]. Other experimental studies have employed this technique to reveal internal injector fluid dynamics [36,37], yet Moon focused on EOI dynamics within a critically controlled and simplified environment. This permitted a more reliable decoupling of the processes governing vapour formation, air ingestion and fuel 'dribble'.

Confining observations to the EOI addresses an important issue since fuel residing and entering the cylinder during and after EOI will not combust efficiently, if at all [28]. This residing fluid will succumb to the evolution of in-cylinder conditions and is expected to carry out complex physical and chemical changes throughout the cycle. Eagle & Musculus [30] used high-speed digital imaging to study the spatial and temporal development of nozzle-residing fuel throughout a full engine cycle. They concentrated on processes in which fuel residing within the nozzle orifices and sac discharged onto the injector surface whilst varying the injector, IP and timing. Their experimental setup suffered from reflections that impeded observation of the fluid behaviour and the optical magnification did not allow the fine liquid structures to be resolved.

Several research groups have used computational fluid dynamics to model the EOI fluid processes [32,34,38]. These techniques often utilise large-eddy simulation framework and employ the volume of fluid method, owing to its ability to track the liquid–gas interface explicitly [39]. These simulations predict a relatively steady-state of flow from the start of needle descent, up until the needle lift falls below the point at which the frustoconical cross-sectional area is below that of the combined orifices [40]. Once this point is reached, flow throttling begins and the pressure inside the nozzle drops rapidly, continuing until the needle becomes seated. The minimum internal pressures are realised, predicted to fall below the vapour pressure of the fuel, inducing cavitation pockets and gas ingestion [31,34,40–42]. The effect is more prevalent at elevated IPs as the greater pressure gradient across the orifice channel leads to extended pressure recovery times [40,41]. The models' predictions for ligament formation and gas ingestion show strong agreements with the experimental observations, gaining well characterised accounts of these phenomena.

It is hypothesised that fuel resides on and within the injector until the subsequent injection event. If true, the fuel must carry out numerous chemical and physical processes due to the highly transient, elevated temperatures, pressures and gas velocities within the cylinder. It is possible that fuel remaining in the injector nozzle is ejected into the cylinder due to these temporal variations [30]. Therefore, extending the optical investigations of the near-nozzle region past the EOI, considering the entire fluid evolution, is essential.

The present study aims to build on the authors' previous work involving multi-hole visualisations of EOI behaviour, in which the dependencies of the fuel discharge on engine operating conditions were elucidated [43,44]. The optical methods employed here achieved greater spatial resolution and illumination homogeneity than prior investigations, permitting analysis of smaller fluid structures and fine intricacies in their behaviours. Statistical knowledge regarding the observed phenomena gave insights into their likelihood of occurrence and

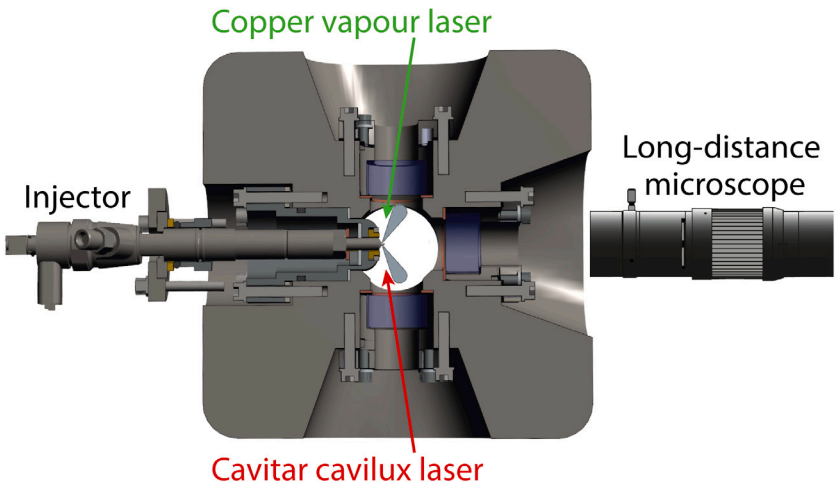

Fig. 1. Schematic diagram of the experimental configuration.

Table 1
Operating conditions, hardware parameters & characteristics.

Parameter	Value
Fuel	n-dodecane
Compression ratio	9:1
Engine speed	500 rpm
Peak motored ICP (target)	5 MPa
Peak ICT (simulated)	650 K
Nozzle tip temperature	405±1 K
Injection pressure	50; 150 MPa
Injection timing	–60; –30, 0, 30°CA aTDC

characteristic onset times with respect to engine operating conditions. To convey the results in the most succinct and useable form, we propose a phenomenological model (Section 3.3) which summarises the key phenomena we observed and their timings throughout a revolution typical of idling/low-load conditions.

2. Methodology

The principal apparatus used in this research was a single cylinder reciprocating rapid compression machine, comprehensively described by Crua [45]. The test-bed was converted from a Ricardo Proteus single cylinder engine into a 2-stroke high pressure spray rig through the removal of the valves and the addition of optical accesses into the combustion chamber (Fig. 1). The cylinder bore was 135 mm with a stroke of 150 mm giving a total engine displacement of 2.2 litres. The large volume (80 mm height, 50 mm diameter) optical chamber reduced the compression ratio to 9:1, so the intake air was boosted to reach a peak motored pressure of 5 MPa. The intake air was intentionally not heated to inhibit combustion. This allowed us to study the influence of other operating parameters without the added complexity introduced by different ignition delays. We must stress that we did perform a similar study under reactive conditions and observed that our results and proposed phenomenological model remained valid. These reactive results, which are beyond the scope of this study, will be presented in a future article.

All tests were performed at low (idle-like) to medium load conditions with an engine speed of 500 rpm and a peak motored ICP of 5 MPa. A thermodynamic model was used to approximate the peak ICT at 650 K. The IP was varied between 50 and 150 MPa to investigate the impact of the in-nozzle conditions around EOI and the injection timings were varied between –60 and 30° Crank Angle (CA) to study the effect of ICP and ICT gradients immediately after EOI. Details regarding the operating conditions and engine parameters can be found in Table 1.

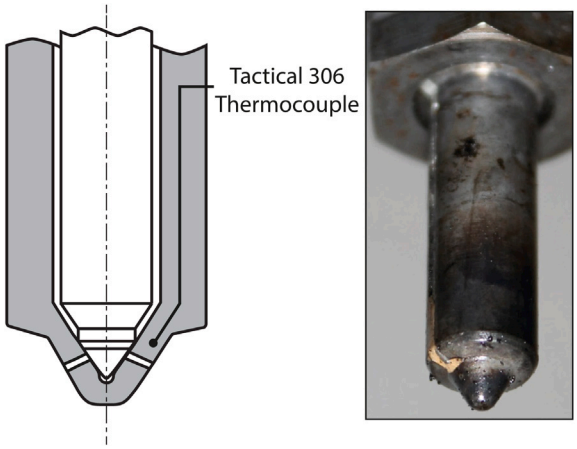

Fig. 2. Diagram of the thermocouple placement for the temperature instrumented Siemens DW10b injector. The thermocouple was embedded down the edge of the nozzle with the probe tip measuring the temperature next to the orifice. It had an accuracy of ±1 K at a rate of 1 reading per cycle.

A single component fuel (n-dodecane) was used so that the processes could be investigated in terms of the fuel physical properties, engendering a more fundamental analysis of the phenomena observed. The fuel was delivered by a Delphi common-rail system, comprising a DFP-3 high-pressure pump rated at 200 MPa and a six Ø145 µm hole Siemens DW10b injector. The injector had a Valve Covered Orifice (VCO) type nozzle, chosen to permit consideration of the orifices independently when the valve is closed, which would not be possible with a sac type nozzle due to the interconnection between the orifices. A piezo-actuating system opened the needle valve, increasing the needle ascent and descent times providing numerous benefits to the spray formation (mentioned in Section 1). This production injector was instrumented with an integrated thermocouple at the nozzle tip, estimating the average surface temperature each cycle (Fig. 2). The in-tank fuel temperature was measured as 32 ± 2 °C but it was too challenging to measure the in-nozzle fuel temperature (which would have been higher due to pump loading). Readers interested in time-resolved measurements of nozzle tip temperatures are advised to refer to our recent article on this topic [46].

By mounting the injector orthogonally to the incident light, it was possible to visualise all of the orifices simultaneously. Fig. 3 depicts the illuminated nozzle with the orifices labelled clockwise from 1 to 6 from 12 o'clock. The light source consisted of two lasers (Fig. 1). Laser 1

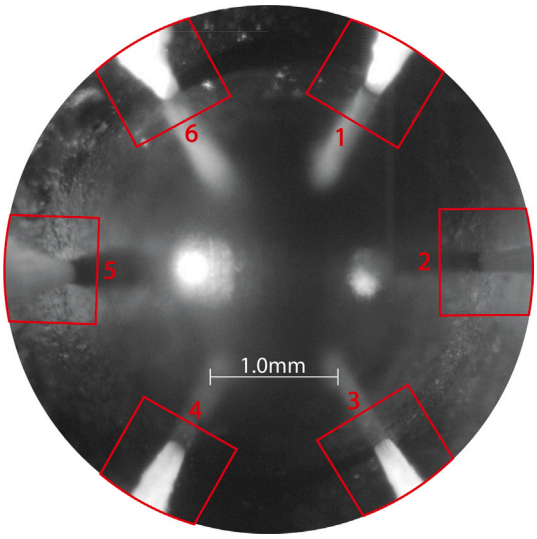

Fig. 3. View of the injector nozzle tip showing the orifice labelling convention used in this article. A scale bar is used to indicate the relative sizes and resolution.

Table 2
Imaging equipment specifications.

Parameter	Value
Camera	Phantom V12.1
Frame exposure time	4 µs
Frame rate	10,000 fps
Image resolutions	704 × 704 pix
Field of view	4.63 × 4.63 mm
Laser 1 pulse	25–30 ns (FWHM)
Laser 2 pulse	100 µs (FWHM)
Scale factor	6.58 µm/pixel

was a CAVITAR Cavilux solid state diode laser was emitting at 690 nm. Laser 2 was a copper vapour laser emitting at 511 nm and 578 nm. The beams were delivered via optical fibres mounted adjacent to the test rig. Laser 1 was controlled via a software interface that subsequently triggered a Quantum-Composer signal generator, relaying another pulse to drive laser 2. The pulse duration of laser 1 exceeded the exposure time of the camera giving exposure control to the camera, set at 4 µs. The high-speed video recordings were obtained by a Phantom V12.1 camera fitted with an Infinity K2 DistaMax long range microscope to significantly increase the magnification. Specifications of the imaging equipment are given in Table 2.

The video recordings depicted the fluid dynamics on and near the injector nozzle surface. Each recording was taken for a full 2-stroke engine cycle at specified operating conditions. Automated image processing were not used to analyse the data due to the highly complex nature of the fluid processes involved during the end of injection. Hence, the video were inspected manually with regard to the various fluid phenomena observed, permitting the frequency and onset times to be collated and analysed. The relative frequency of each fluid phenomena was calculated per cycle per orifice, so normalised against the total cycles analysed and the 6 orifices on the injector. The frequencies and onset times were compared when varying the IP between 50 and 150 MPa, and the injection timing between –60 and 30°CA, enabling elucidation of the dependencies on in-nozzle and in-cylinder conditions.

3. Results

3.1. Outline

The following section outlines the near-nozzle and nozzle-bound fluid processes typical of a diesel injector under low (idle-like) to medium load operating conditions. The phenomena are presented in a chronological order with regard to their onset times. The Start Of Injection (SOI) and the main injection phases are not described here as they have been extensively characterised in other studies [2,47–49]. Visual inspection of the video recordings showed SOI and main injection behaviour in agreement with our previous findings [49].

Note that contrary to the literature we avoid using the term ‘dribble’ to describe some of these phenomena. While the term is often used in the literature to describe fuel discharge that occurs *immediately after* an injection event, it is also commonly used to describe all fuel discharges that occur *at any time* during the engine cycle [30]. While our decision aims to avoid further confusion, it is also a consequence of this research identifying a broad range of mechanisms that led to uncontrolled fuel overspill, over many different timescales. In our view, these phenomena require a more detailed taxonomy which we aim to rationalise in the rest of this manuscript.

Each subsection describes a different phenomena, evaluating its frequency, timing and visual characteristics. Further comparison are given against varied operating conditions for exploration into the underlying mechanisms. Image sequences for each of the phenomena are provided in Fig. 4, ordered chronologically by their onset times. For convenience a short description of each event is listed below with the letters and names interlinking them to the measured timings (Fig. 5) and frequencies (Fig. 6):

(A) **Splashback**
A spray wetting mechanism occurring during the end of injection [50]. The highly transient behaviour of the fuel structures and large localised gas velocities cause a considerable volume of droplets to divert back towards the nozzle, subsequently impinging to form surface-bound fuel films (Supplementary Video S2).

(B) **Ligament retraction**
A spray wetting mechanism occurring during the end of injection event [27,31,35,50,51]. A low inertia ligament at the end of the injection event maintains adherence to the nozzle surface. The surface tension and internal cohesive forces cause the ligament to retract back towards the nozzle, resulting in the formation of a fuel film (Supplementary Video S3).

(C) **Vapour expulsion**
Immediately after the end of injection vapour can be observed seeping out of the orifice (Supplementary Video S4). It is believed to result from heat transfer to a thin film on the orifice wall, causing it to vaporise.

([D) **Expansion overspill**
Fuel emerges from the orifices due to equalisation with the ICP during the expansion stroke [30,43,44,52]. This equalisation leads to an expansion of vapour/gas bubbles trapped within the fuel inside the orifices. This event is the biggest contributor of fuel deposition on diesel injector nozzles (Supplementary Video S5).

(E) **Orifice bubble**
Overspill is frequently interrupted by the expulsion of trapped gas [43]. Gas becomes encapsulated by fuel films covering the orifice exit, forming a bubble that can be wider than the orifice diameter (Supplementary Video S6).

(F) **Bubble collapse**
The orifice bubble (*E*) becomes too large to maintain its shape. Small instabilities induced by the engine environment instigate its collapse (Supplementary Video S7). The bubble membrane retracts into a large ligament and large droplet(s), released into the cylinder.

(G) **Surface bubbling**
The formation, growth and coalescence of microscopic bubbles within a fuel film [43]. Identified by the increased pixel intensities induced by a heightened scattering from the gas–liquid interfaces (Supplementary Video S8).

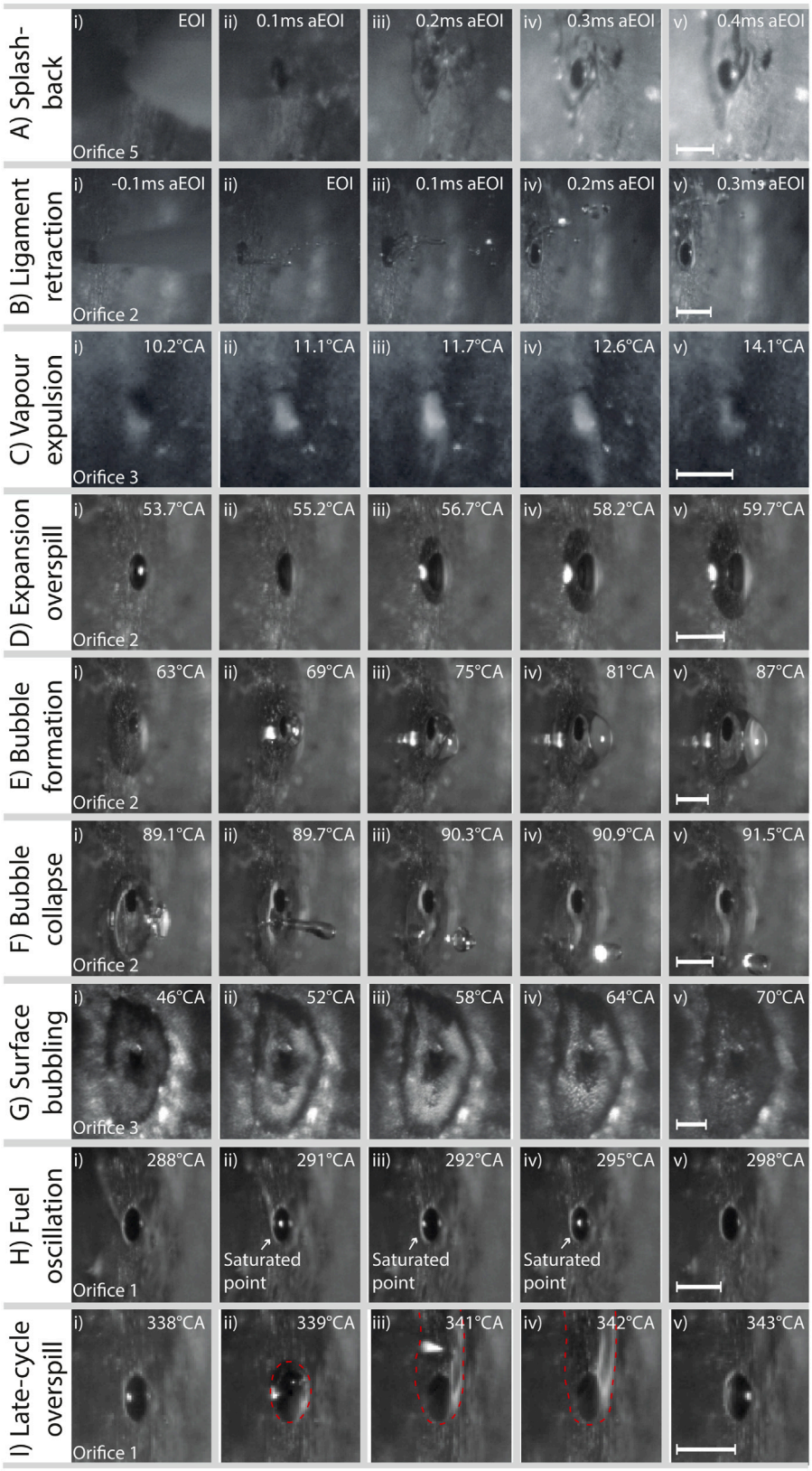

Fig. 4. Image sequences for each of the phenomena identified, labelled with letters corresponding to a short description in the text (Section 3.1), along with graphical depictions (Fig. 8). The timings and frequencies of the phenomena can be found in Fig. 5 and Fig. 6 respectively. A scale is given by a white bar in the final image of each sequence, with a length on 0.2 mm. Videos of these phenomena can be found online at https://doi.org/10.1016/j.fuel.2021.122208.

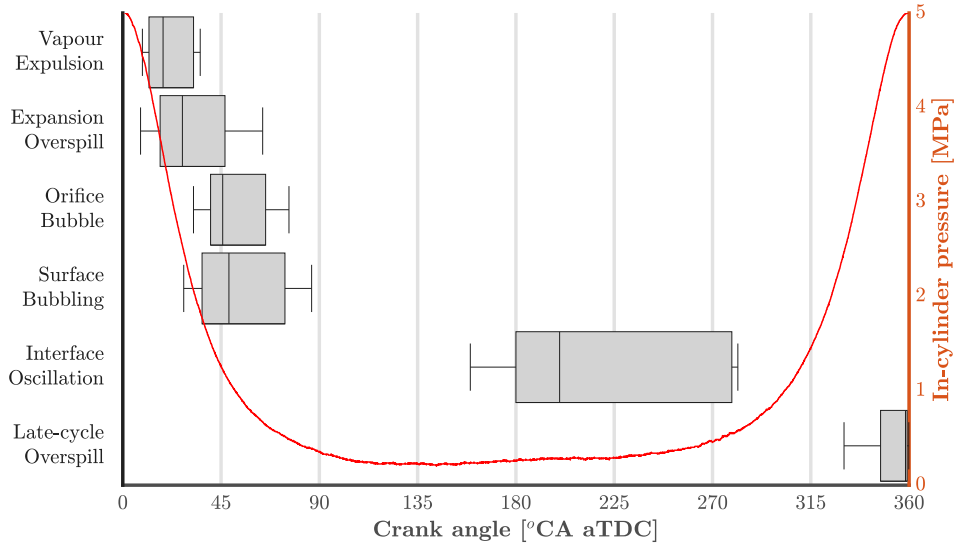

Fig. 5. Box plots giving the spread in onset time for each of the phenomena observed for a TDC injection, depicted in Fig. 4. Since spray wetting occurs immediately after the injection event the onset time is shown by a single line. For the other phenomena box-plots are used. The central box-plot line gives the median, the box's bounds give the lower–upper quartiles and the whiskers show the minimum and maximum times observed. The figure does not depict to the frequency of the phenomena, which is given in Fig. 6.

Table 3
Characteristic onset timings of the phenomena in °CA aTDC. Data for both 50 and 150 MPa injection pressures has been combined since no significant differences were found. They are displayed with regard to the injection timing, varied between –60 and 30°CA aTDC. The majority of the phenomena occur during the expansion stroke regardless of the injection timing. Lettering is used to relate the phenomena to the image sequences in Fig. 4 and the graphical interpretations in Fig. 8. Some phenomena are not included as their frequencies could not be accurately measured.

Phenomena	Injection timing [°CA aTDC]			
	–60°CA	–30°CA	0°CA	30°CA
(C) Vapour expulsion	n/a	26°	22°	44°
(D) Expansion overspill	40°	35°	36°	59°
(E) Orifice bubble	57°	52°	58°	71°
(G) Surface bubbling	49°	52°	54°	67°
(I) Late-cycle overspill	355°	327°	352°	352°

(H) **Fuel oscillation**
The oscillation of a gas–liquid interface in and out of an orifice. Identified by the motion of a small saturated intensity region, which results from a reflection of the lasers off the interface (Supplementary Video S9).

(I) **Late-cycle overspill**
Fuel overspilling out of an orifice at the end of the engine cycle [30]. The phenomena is similar to expansion overspill but occurs during a rise in ICP on the compression stroke, potentially due to increased local gas velocities (Supplementary Video S9).

The observed onset times for the fluid phenomena were recorded and the medians and spread were calculated. The onset results are displayed in the form of box plots in Fig. 5, listed in chronological order from top to bottom. It should be noted that these results are for the onset of the events and do not represent their duration or frequency. For instance, the expansion overspill has a much larger frequency and duration than the interface oscillation, yet the interface oscillation has a much larger variation in its onset time giving it greater presence in the figure. The onset timings are critical for the evaluations made in each of the subsections (Fig. 5).

The majority of event onset times are situated in the first half of the expansion stroke, emphasising the strong impact of the ICP drop during this time (Fig. 5). As the onset times are clustered towards a short period, there is inevitably a large amount of overlap. However, a few rules should be considered. Vapour expulsion always occurs before overspill and never after, yet the overspill is not dependent on the presence of vapour expulsion. Surface bubbling and orifice bubbles will not develop if an overspill event has not previously occurred. Bubble collapse would obviously be dependent of an orifice bubble and all orifice bubbles subsequently collapse.

In order to elucidate the primary dependencies of the phenomena described in the proceeding subsections, it is crucial to decouple the effects of ICP, gas flow and ICT. This was achieved through variation of the injection timing between –60 and 30°CA after Top Dead Centre (aTDC), combined with two distinct injection pressure test points. By isolating the ICP evolution, in particularly the pressure change during EOI, it was possible to evaluate the dependence of the fuel phenomena on the instantaneous in-cylinder pressure as well as its rate of change. The IP variation between 50 and 150 MPa provided diverse internal nozzle dynamics during and after the EOI. Higher IPs are known to give increased momentum to the fluid leaving the nozzle, as well as causing more gas ingestion and lower internal pressures immediately after the injection event [34,40–42]. The method permitted decoupling of the in-nozzle conditions on the phenomena in relation to the in-cylinder conditions. The test-points were specifically chosen to elucidate the dependencies of the underlying processes on the near-nozzle/internal conditions, ultimately unravelling the primary mechanisms through processes of induction, deduction and elimination.

The impact of varying the injection timing on the phenomena's onset timing is very small for all of the phenomena investigated (Table 3). All of the processes are shown to be exclusive to the expansion stroke i.e. <180°CA aTDC, apart from the late-cycle overspill which consistently occurred at the end of the following compression cycle (Table 3). This indicates that the onset times are primarily dependent on the temporal evolution of in-cylinder conditions and that they do not occur at constant delays after EOI. This demonstrates that the underlying processes that result in the phenomena shown in Table 3 are dependent on the *derivative* of the in-cylinder conditions and not their instantaneous value.

In addition to the onset times, the frequencies of occurrence for each of the phenomena are also important in assessing the impact of the events, given in Fig. 6. It specifically focuses on the distinct differences in occurrence rate when varying the IP during TDC injections. The frequency and onset times have been documented manually with regard to specific visual traits of the phenomena (eg. sudden differences in pixel intensities in a region, or the motion/appearance of a high intensity regions). It is possible that errors may infrequently occur from

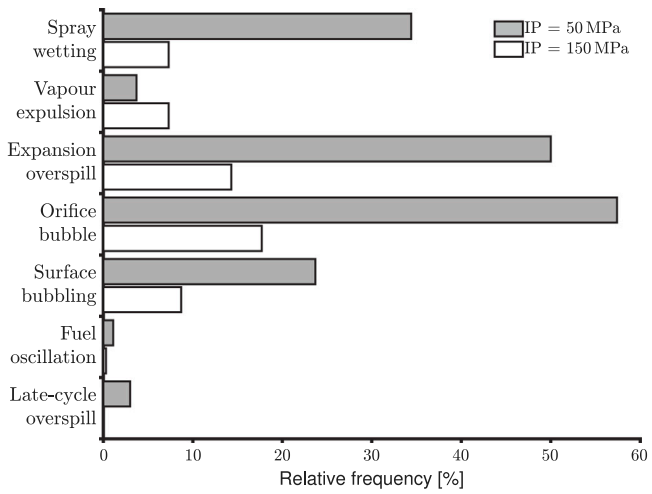

Fig. 6. Bar plots of the relative percentage frequencies for the phenomena observed, per orifice per cycle. The results are for injections at top dead centre for 50 and 150 MPa injection pressure. The phenomena relate to the image sequences in Fig. 4 and the graphical interpretations in Fig. 8. All phenomena occurred more frequently at the lower injection pressure, except for the vapour expulsion.

visualisation problems, like gas or droplets obscuring the view of a phenomena within a frame, yet the maximum manual error resulting from these problems will always be less than ±0.6°CA (2 frames or 0.2 ms).

Unlike the variation in injection timing, changing the IP from 50 MPa to 150 MPa had a considerable effect on all of the phenomena observed (Fig. 6). The majority of phenomena are notably less frequent when the IP is increased, believed to be governed by the inertia of the EOI fuel dictating the degree of gas ingestion and the volume of fuel that resides within the orifices [42]. The vapour expulsion is the only phenomena to increase in frequency with the IP indicating a possible dependency on the in-nozzle pressure drop at the EOI [34,40].

The frequency, onset data and fluid behaviour is discussed further in each subsection, specifically focussing on each phenomena (Section 3.2). Image sequences are given for each phenomena described in Fig. 4. Investigation of the timings and visual characteristic has permitted the development of a phenomenological model that conceptually depicts each event with the characteristic timings (Section 3.3). The subsection names relate them to the graphical annotations.

3.2. The post injection phenomena

3.2.1. The end of injection

The flow becomes throttled when the gap between the needle and its seat drops below the total areas of the combined orifices [34]. At this point, the internal nozzle pressure rapidly decreases and the flow becomes prone to cavitation behaviour [32,34]. As the needle descends further, eventually relocating in its seat, the flow's inertia rapidly dissipates and atomisation of the emerging spray is inhibited. It is clearly shown in Fig. 7 that the spray dynamics observed during this period are strongly dependent on the IP. The larger dispersion angle and reduced overspill period for the 50 MPa injection indicate the direct relationship with the flow's inertia and inertial dissipation at any instance. If the inertia is too low to permit an atomisation regime, the spray will contract into a singular column surrounded by orbiting droplets [43]. However, when atomisation is achieved, the dispersion angle of the spray will increase as the inertia gradually reduces, decreasing the distance between the spray periphery and nozzle surface (Fig. 7).

As the flow throttling increases and atomisation is inhibited, the droplet diameters increase [53] causing the release of large, slow moving fluid structures into the cylinder. These structures maybe too large to undergo complete combustion and have the potential to produce by-products that could contribute towards both engine-out emissions and coking. Any fuel that does not combust may later get drawn into the exhaust where it would directly contribute towards UHC emissions (pre after-treatment).

It has been shown both numerically and experimentally that during the end of injection event in-cylinder gas is ingested into the nozzle [32,34,41]. This is because the inertia of the fuel causes it to continue exiting the nozzle after the needle valve is closed. Since the in-nozzle space is not refilled with fresh fuel, the pressure significantly drops promoting cavitation. In-cylinder gas is subsequently ingested to equalise the in-nozzle pressure with that of the cylinder, yet the gas temperature is high and may contain deposit precursors. Fig. 7(2) shows a gap between the emerging spray and the orifice wall. It is believed that this gap represents a passage in which in-cylinder gas would be able to enter the nozzle. The process of gas ingestion has utmost importance in consideration of the subsequent phenomena, since it determines the composition of the contents residing in the nozzle after the injection event [42].

The end of injection process was completed within 0.6 ms after the end of injection trigger for our test conditions. The duration shows a high dependence on the operating conditions, with longer durations at lower IPs. An image sequence for a typical end of injection event is given in Fig. 7. The frequencies and timing variation when adjusting the injection angle can be found in Fig. 6 and Table 3 respectively. The characteristic duration of the end of injection was approximately 0.6 ms with a high dependency on the injection parameters.

3.2.2. Spray wetting

The impact of the in-cylinder conditions becomes more pronounced towards the end of injection, identifiable by the motion of the large liquid structures (Figs. 7B,C). At this time (0.2 ms aEOI), fuel frequently wets the nozzle surface through two potential mechanisms: splashback and ligament retraction.

A pattern regarding the critical conditions to induce these EOI spray wetting phenomena has not been found, illustrating the highly transient, multi-dependency nature of the EOI fluid dynamics, already highlighted in some experimental studies where significant shot to shot variations were observed [31]. Both phenomena produce a considerable volume of liquid deposition on the nozzle surface which proceeds to spread across the nearby area. The resulting fuel film creates a localised fuel rich region that, despite being present at the end of the combustion event, will neither react nor completely evaporate during this time. The high ICP increases the vapour saturation temperature [54], reducing the vaporisation rate, supported by visual inspection of the fuel films residing into the second stroke (Supplementary Video S1). The film acts as a region which may trap combustion by-products or aid deposit forming reactions [9,17]. The films will eventually evaporate later in the cycle(s), shown by the reduction/total removal of surface-bound fuel by the end of the cycle (Supplementary Video S1), releasing un-reacted fuel vapour into the cylinder that is likely drawn into the exhaust.

The two modes of spray wetting identified are visually presented (Figs. 4A–B) and detailed below:

Splashback

At the end of injection the dispersion angle is at its maximum, reducing the distance between the EOI liquid structures and the nozzle (Fig. 7). The inertia of the droplets is low and they are large which increases susceptibility to interactions with the in-cylinder gas flow. High turbulence in the nozzle causes increased helical behaviour [27]. Tangential flow vectors become more pronounced as the flow decelerates, creating a swirling fluid column at the centre of the jet [55]. Positive tensile stress and local velocity fluctuations increase with the turbulence in the flow. Since the flow inside the nozzle is already thought to contain significant turbulence [34,56], highly transient two-phase

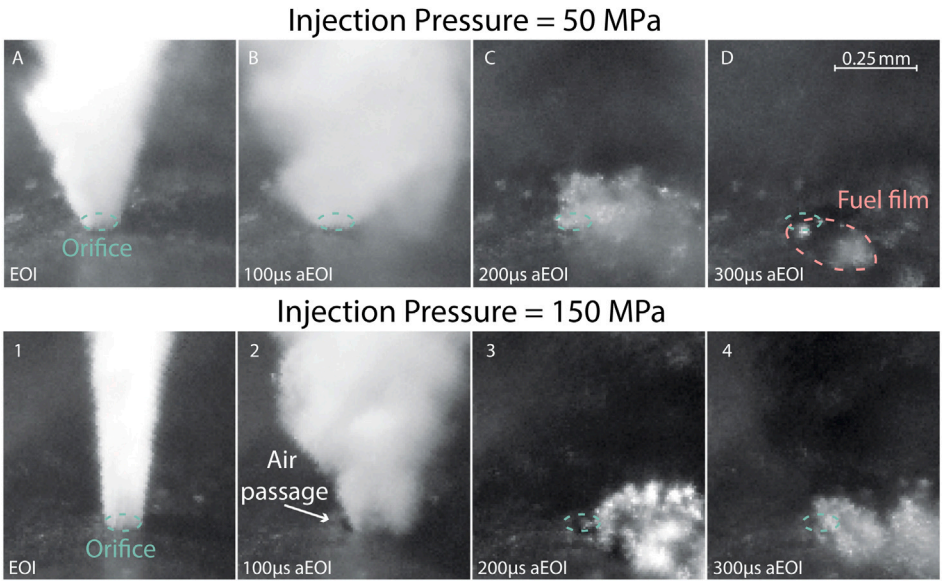

Fig. 7. Two image sequences showing the collapse of the spray at the EOI for both 150 and 50 MPa IPs. The 50 MPa IP images are labelled from A–D and from 1–4 at 150 MPa IP. D shows a resulting fuel film from droplet impingement. Image 2 shows a gap at the side of the emerging spray which is thought to result from gas being ingested into the nozzle as the fuel leaves [27].

interactions take place that develop as the flow enters the cylinder. The sudden deceleration of the spray as the needle becomes seated creates an increased diversity in droplet trajectories and a greater dispersion angle. The end of injection dynamics cause droplets to be diverted back towards the nozzle, wetting the nearby surface (Fig. 4A). Although injection and combustion processes are highly controlled, the numerous factors and dependencies governing this event lead to significant shot to shot variations.

Ligament retraction Fig. 4B depicts the process of spray wetting through the retraction of an EOI ligament. Once the momentum of the fuel spray has sufficiently dropped, the exiting fuel forms large, slow moving structures that maintain adherence to the orifice walls (provided breakup is not dominated by turbulent forces, as in the case for splash-back). The ligaments released as the injection comes to an end will either split from the orifice adhering fuel, or the combined surface tension and internal cohesive forces will cause it to retract back towards the nozzle, collapsing onto the nearby surface. It is unlikely that the retraction moves directly back towards the surface as the size and low inertia of the structure make it susceptible to interactions with the in-cylinder gas. A sidewards collapse generally occurs in the direction corresponding to the local gas flow field.

Dependence on injection pressure

The spray wetting phenomena discussed are collectively referred to as spray wetting since distinguishing them from each other can be challenging. They are grouped together under the 'Spray wetting' descriptor in Fig. 6.

The results in Fig. 6 are consistent with our previous investigation [44] in which the initial evolution in wetting was tracked. The increased frequency at lower IPs provides evidence that the wetting process is strongly dependent on the fuels inertia (Fig. 6). The increased inertia of the EOI fuel when injecting at higher pressures will reduce the dispersion angle, minimising the distance between the spray periphery and the nozzle surface, hindering droplet impingement. Any slow moving structures at the end of injection will have increased axial momentum, inhibiting their adherence to the surface. Furthermore, the needle descent is dependent on the IP, thus a higher IP will reduce the time spent within the end of injection phase.

An image sequence for a typical spray wetting event is given in (Fig. 4A–B). The frequencies and timing variation when adjusting the injection angle can be found in Fig. 6 and Table 3 respectively. The characteristic onset time found for the investigated conditions was EOI–0.6 ms aEOI (Fig. 5).

3.2.3. Vapour expulsion

After the EOI dynamics there is a delay in which there is no activity in or around the orifices, lasting approximately 7 ms when injecting at TDC, and longer when injecting before TDC. The needle valve is expected to be completely sealed, thus preventing any displacement of fuel between the orifice of this VCO nozzle. The contents of the orifice holes is a mixture of liquid fuel, vapour fuel and ingested gas [34,41]. Fuel vapour expulsion can be identified when white plumes seep from the orifices approximately 21°CA aTDC (Fig. 4D). The fuel vapour expulsion never occurs after the overspill event (Section 3.2.4) although overspill regularly develops after the vapour expulsion. The emerging gas is identified as vaporised fuel due to its cloudy appearance (Fig. 4D). Independently of the injection timing, the vapour expulsion always occurred at a similar timing during the expansion stroke (Table 3). The result indicates that the vapour emerges into the cylinder as a results of the ICP drop. Equalisation causes the gas and vapour content in the orifices to expand and eventually emerge out of the nozzle [44].

The formation of vapour within the orifices can be explained by the evaporation of thin films on the orifice walls through heat transfer from the nozzle. Fig. 6 gives a low frequency of vapour expulsion for all conditions tested, possibly due to re-condensing of the vapour when contacting other fuel structures within the orifice. Conversely motion of the vapour and surrounding gas may create a very lean mixture that was undetectable by the imaging system. The frequency of the vapour expulsion was considerably reduced when injecting before TDC which would give the vapour an extended period to either re-condensate or mix with the surrounding gas prior to being forced out of the orifice by the in-nozzle gas expansion (Table 3).

An alternative hypothesis is that of air, dissolved in the pumping system, precipitating out of the residing fuel. However, the precipitating air would not have the condensing, mist-like appearance that is observed in the HSV data because its vapour saturation pressure is too low. Furthermore, the high pressure at TDC would inhibit the precipitation of the gas until later in the cycle (inferred through Henry's law).

Unlike for all other phenomena observed, the frequency was considerable reduced at the lower injection pressure test points (Fig. 6). It

is likely that this is a result of a lower volume of fuel residing within the nozzle at higher injection pressures due to increased fuel inertia, as shown throughout this study. A thin film residing on the nozzle wall will evaporate more rapidly than a slug of fuel partially filling the orifice, as the surfaces available for heat and mass transfer are significantly increased.

An image sequence for a typical vapour expulsion event is given in Fig. 4C. The frequencies and timing variation when adjusting the injection angle can be found in Fig. 6 and Table 3 respectively. The characteristic lower–upper quartiles of onset times found for the investigated conditions was 13–32°CA aTDC (Fig. 5).

3.2.4. Expansion overspill

Overspill is a term used to describe the processes in which nozzle residing liquid emerges from the orifices between injection events. The emerging fluid forms fuel films on the nozzle surface surrounding the orifices and is thought to contribute to the formation of external deposits [17]. The fuel may evaporate later in the cycle, subsequently being drawn into the exhaust and directly contributing towards engine-out UHC emissions.

The phenomena has been identified at multiple timings throughout the engine cycle but most commonly on the expansion stroke. It is believed that all overspill events that take place during the expansion stroke are elicited by the same underlying mechanisms, referred here as 'expansion overspill'. Overspill later in the cycle is referred as 'late-cycle overspill', as it likely arises from different mechanisms, and described in Section 3.2.8. Expansion overspill was the primary cause of fuel deposition for all the conditions we tested, as observed in our previous studies [43,44]. Our previous research showed that fuel overspills during the expansion stroke due to the expansion of nozzle trapped gas, forcing the residing fuel to emerge out of the nozzle. The conclusion is further supported by the results in this study as all of the overspill events occurred around the middle of the expansion stroke when the ICP drop is peaking, independently of injection timing (Table 3). Injecting at –60°CA aTDC caused a slight retardation in the onset time (Table 3). Since it is established that the fuel emerges due to the expansion of ingested gas and the ICP at –60°CA will be lower than that at –30°CA or TDC, it is possible that the in-orifice gas from an earlier injection will experience less expansion, causing the observed retardation.

The overspill was considerably suppressed at higher IPs (Fig. 6). The limited literature on post-injection discharge from the orifices shows little dependence on IP [30]. The amount of fluid emerging from the orifices should depend on the ratio of gas–liquid volume inside the orifice after EOI and, as discussed in Section 3.2.1, the ratio is dependent on the IP. Increased gas volume in the orifice would supply a greater force to dislodge the fuel, but if there is limited fuel in the orifice the overspill cannot occur. The results show that higher IPs reduce the amount of fuel in the orifice, ultimately reducing the frequency of the overspill. However, since only two IPs were tested a comprehensive relationship cannot be given.

An image sequence for a typical expansion overspill event is given in Fig. 4D. The frequencies and timing variation when adjusting the injection angle can be found in Fig. 6 and Table 3 respectively. The characteristic lower/upper quartiles of onset times found for the investigated conditions at TDC injection timing was 17–47°CA aTDC (Fig. 5).

3.2.5. Orifice bubble formation and collapse

After the injection event the nozzle is filled with a mixture of residing liquid fuel, ingested gas and vaporised fuel. The previous Section 3.2.4, in addition to previous research [43,44], provides evidence that the orifice-trapped previously ingested gas expands during the pressure drop on the expansion stroke, forcing fuel out of the nozzle, forming surface-bound films. The films cover the orifices, yet orifice trapped gas is also forced out of the orifices inbetween fuel emergence. If the emergence of gas follows the formation of a film, covering the orifice exit, the film will encapsulate the emerging gas in the form of a bubble (Fig. 4E). If the bubble maintains its position at the orifice exit, subsequent emerging gas pockets may coalesce with the orifice bubble, increasing its size. Further growth occurs as the ICP drops and the gas contained in the bubble expands (Fig. 4E).

The event provides clear evidence that there is expanding gas within the orifices mixed with the fuel, supporting the statements regarding expansion overspill. It is closely associated with the overspill, since the emergence of the gas filling the bubble has the same underlying mechanism: the expansion of orifice-trapped, previously ingested gas, dislodging the in-orifice contents. This is reflected by the onset timing results when varying the injection timing (Table 3). Similarly to overspill, the bubble formation occurs exclusively on the expansion stroke, independent of injection timing, indicating its dependence on the ICP drop. There is little variation in the onset times, with the largest difference being a small delay when injecting at –60°CA. It is possible that the lower pressure of the in-cylinder gas being ingested when injection at –60°CA results in less expansion during the ICP drop, causing the small delay before onset.

The bubble formation and overspill also have similar relationships with the IP (Fig. 6). The frequency of occurrence is much greater at lower IPs and lower IP is conducive of high fuel-gas ratios in the orifices. It then follows that the frequency of bubble formation is promoted by a high fuel-gas ratio, possibly ensuring that the fuel film is present to encapsulate the gas on expulsion. However, the frequency is measured and not the total gas volume thus, a higher IP could produce larger but less frequent bubbles.

As an orifice bubble grows, the encapsulating liquid membrane thins and the ratio between internal and outer pressures increases [57]. Consequently, susceptibility to instabilities induced by the surrounding environment escalates. When the surface tension no longer prevails over the environmentally induced instabilities (primarily instigated by nearby in-cylinder gas flow), the bubble's membrane will tear, resulting in its collapse.

The surface tension causes the fuel sheet to retract either towards the contacting surface-bound film, or a thicker region of the sheet, normally towards the tip (Fig. 4F*i*). Fuel retracting towards the surface will increase the volume of the film at the base of the bubble, whereas fuel retracting towards a central point will form a large airborne ligament (Fig. 4F*ii*). The surface tension and internal cohesive forces within the ligament result in further contraction. In the pursuit of equilibrium, the fuel retracts into one or several droplets, dependent on the size and shape of the original ligament produced (Fig. 4F*iii*). Release of the gas previously contained within the bubble creates a small, localised pressure wave that frequently interacts with the droplets, projecting them into the cylinder. The airborne droplet gives no indication of this gas interaction (Fig. 4F), permitting enhanced visualisation.

To the best of our knowledge neither orifice bubbles nor their collapse have been reported in the literature, yet these phenomena show significant importance, particularly due to the resulting formation and projection of large airborne fuel structures. The droplets form post combustion and are likely to be drawn into the exhaust where they will contribute towards engine-out emissions. If instead they impinge on nearby surfaces they will provide a transport mechanisms for deposit precursors and acute regions that may aid deposit formation reactions [17].

An image sequence for a typical orifice bubble event is given in Fig. 4E–F. The frequencies and timing variation when adjusting the injection angle can be found in Fig. 6 and Table 3 respectively. The characteristic lower/upper quartiles of onset times found for the investigated conditions at TDC injection timing was 38–75°CA aTDC (Fig. 5).

3.2.6. Surface bubbling

Fuel films are present on the nozzle surface during the expansions stroke due to the fuel deposition (described in Section 3.2.2) and expansion overspill (described in Section 3.2.4). Surface bubbling is a term used to describe the process of small bubble formation, growth and coalescing within surface-bound fuel films that were formed during the end of injection and overspill events.

The fuel films are initially clear, appearing darker than the surrounding surface as the smooth liquid–gas interface reflects light away from the camera (Fig. 4G*i*). A notable increase in pixel intensities arise as micro-bubbles form within the film, scattering light in all directions by reflection/refraction off the gas–liquid interfaces. The proportion of light scattered into the imaging path becomes significantly greater, being perceived as higher pixel intensities within the bubbling region (Fig. 4G*ii*). The cloudy film develops into distinguishable bubbles as the gas pockets grow and coalesce, giving the appearance of nucleate boiling (Fig. 4G*iii*). The bubbles tend to situate in the thickest part of the film, away from the film periphery and orifice, appearing to maintain an attachment to the surface. The bubbles break when they reach a size approximated between 5 and 20 μm, until only a few remain (Fig. 4G*iv*).

Four potential mechanisms for surface bubbling have been conceptualised and explored:

- Microscopic bubbles are formed within the orifice and are transported onto the surface by the overspilling fuel.
- Heat transfer between the nozzle surface and fuel film causes boiling at the solid–liquid interface
- Air dissolves into the fuel during passage through the fuel pumps. The gas then precipitates out of the fuel as the ICP drops.
- As the fuel film spreads across the nozzle, it traps microscopic pockets of gas in small surface crevices. The gas then expands and coalesces as the ICP drops.

Surface bubbling was explored in a previous investigation with the same potential mechanisms explored [43]. It was concluded that the surface bubbling was due to microscopic bubbles being transported out of the nozzle with the expansion overspill, then expanding as the ICP dropped. However, in the current investigation the phenomena are still observed when the film is entirely composed of spray deposited fuel and not overspill, suggesting a different mechanism is involved. Furthermore, the visual behaviour of the bubbles is significantly different. The bubbles observed in our previous investigation reached sizes more than 10× larger than those observed here with their initial sizes also being considerably larger. Also, contrary to the past observation, the bubbles do not move with the fuel film, preserving an attachment to the nozzle's outer surface. The operating conditions in the two investigations are considerably disparate (increased IPs, ICTs and ICPs being used here with a single component fuel rather than diesel), making it reasonable to compare and consider the two investigations independently.

The possibility of surface boiling being the underlying cause of film bubbling was previously studied, yet reliable conclusions were challenging since a multi-component fuel (diesel) was used [43]. Boiling was refuted for one of the lightest components of diesel (Octane), but only for the onset timing which bubbling was first identified; not for the bubbling occurring later in the cycle. For the current study the likelihood of boiling in the surface-bound films is explored by taking the minimum ICP during the cycle, found to be 0.12 MPa, and obtaining the corresponding vapour saturation temperature (for n-dodecane), given to be 627.5 K [54]. The mean nozzle temperature was 405 ± 1 K for the entire cycle, (expected to be lower during periods of minimum ICP) and the simulated gas temperature for the median onset time of 50°CA was 407 K. Both of these values are significantly lower than the minimum required vapour saturation temperature, hence surface boiling is refuted for any possible timing in the cycle.

The precipitation of dissolved air is reliant on Henry's law, stating "the mass of a dissolved gas is proportional to its partial pressure in the gas phase" [58]. Dissolving the gas into the fuel would most likely occur within the fuel pumps (due to the high pressures achieved), ergo a higher IP should relate to more dissolved gas. Unfortunately, the frequency of occurrence is also dependent on the film volume, and the frequency and volume of the film is more higher at lower IPs (Fig. 6 and [44]). Hence, the frequency data cannot be used in the analysis. The 50°CA aTDC median onset time corresponds to an ICP of 2.21 MPa and an ICP drop of approximately 25× from TDC. Calculations made using data from [59] show that the mass fraction of air that can be dissolved in dodecane drops from 0.013 to 0.003 air_g/$dodecane_g$ between TDC and the characteristic onset time. This large decrease in air solubility could explain why the surface film first becomes cloudy, as this is what would be observed if dissolved air became supersaturated prior to the onset of precipitation. Consequently, precipitation of dissolved gas is a potential surface bubbling mechanism but more evidence is required for a conclusive theory to be drawn.

Crevice trapped gas expansion is the remaining mechanism to be explored yet no solid evidence was found from the conditions investigated to either refute or support this hypothesis. Since there is enough evidence to refute 'boiling' and 'overspill transport', it can be said that 'gas precipitation' or 'crevice trapped gas expansion' are the two most likely mechanisms. Further research is needed to confirm the origin of this phenomenon, possibly using degassed fuel samples, and variations in nozzle surface texture to promote/hinder trapped gas.

An image sequence for a typical surface bubbling event is given in Fig. 4G. The frequencies and timing variation when adjusting the injection angle can be found in Fig. 6 and Table 3 respectively. The characteristic lower/upper quartiles of onset times found for the investigated conditions at TDC injection timing was 40–65°CA aTDC (Fig. 5).

3.2.7. Film interface oscillation

After the end of the expansion stroke there is very little activity in and around the orifices until the following cycle. However, fuel can occasionally be observed moving in and out of the orifices by the displacement of a high intensity reflection from the liquid–gas boundary (Fig. 4H). The phenomenon is thought to be a result of the high velocity in-cylinder gas motion during the compression stroke, leading to a pressure drop in the vicinity of some orifices. Since the nozzle is a VCO type, the orifices are not connected through a sac, and therefore this effect cannot be due internal sloshing from differential pressure fields along the perimeter of the nozzle (such as those noted by Eagle & Musculus [30]).

Manually documenting the oscillation events gave characteristic lower–upper quartiles of onset times between 180–81°CA bTDC (Fig. 5). Occurrence frequencies of 0.3% and 1.1% were obtained for 50 and 150 MPa IPs respectively Fig. 6. The rarity of this phenomenon reduces the reliability of the correlations identified.

Nevertheless, these observations provide some new information regarding the in-orifice contents prior to the subsequent injection. The oscillation must be caused by compression and expansion of the in-orifice contents, yet the fuel is relatively incompressible. Therefore gas must reside within the nozzle throughout the entire cycle, trapped behind the fuel. Since a liquid fuel interface is identified within the orifices during the compression stroke and both expansion overspill and interface oscillation is observed for the same orifice of the same cycle, the expansion overspill event does not always remove all of the fuel from the nozzle. The residing fuel is in the liquid phase and because the pressure is increasing (thus increasing the vapour saturation temperature) it should remain as a liquid until the subsequent injection, impacting the SOI event [49].

We can anticipate that the fluid motion would be more pronounced with sac nozzles, but for the present study of a VCO nozzle there were no incidences of film formation as a result of the oscillating motion. Any spilling on the compression stroke happened later on and closer to TDC, as described in the subsequent subsection.

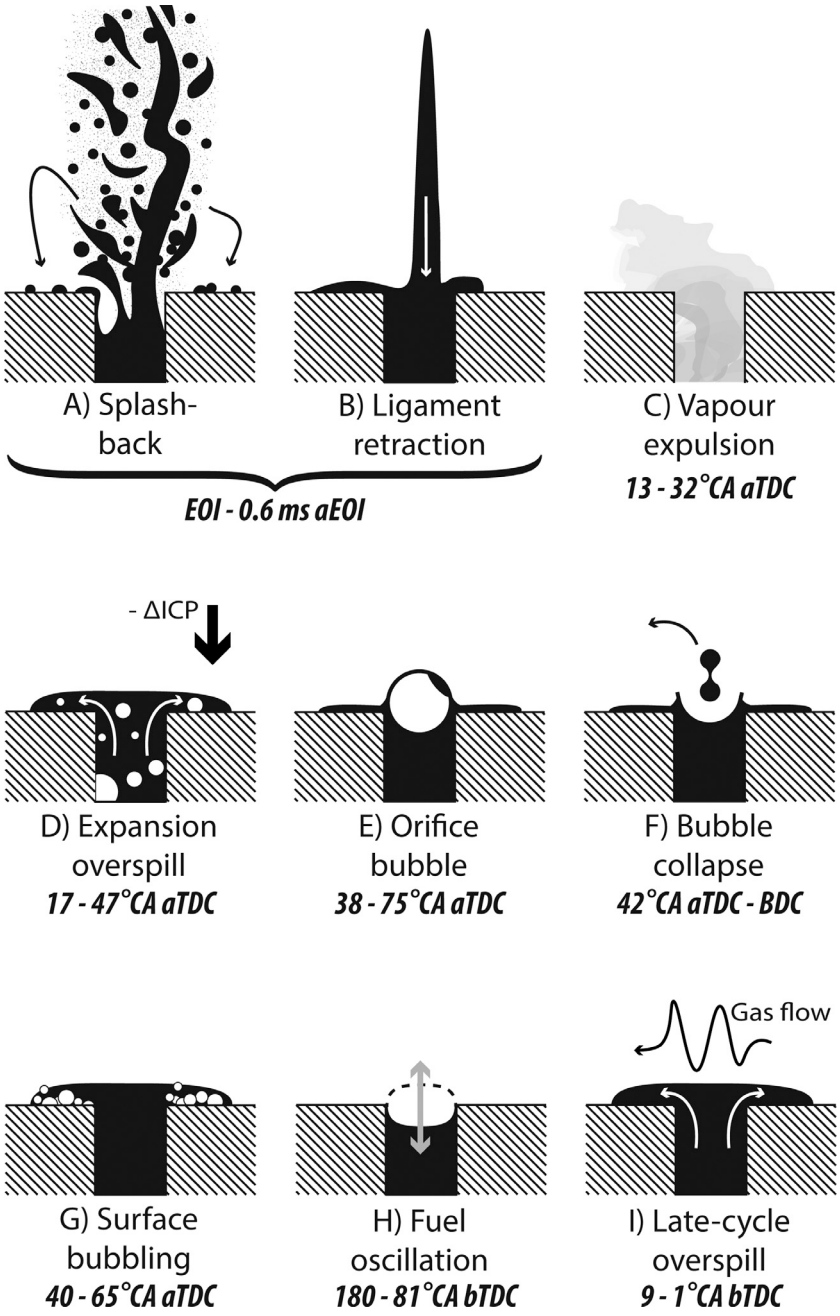

Fig. 8. A conceptual model for the near-nozzle fluid dynamic processes shown in Fig. 4. The graphical depictions of phenomena are presented in a chronological order with focus on the behaviour within the near-nozzle region and the orifices during end of injection. Their names and labels correspond to the previous subsections/image sequences they represent with the lower–upper quartiles in onset times given in Fig. 5.

An image sequence for a typical film oscillation event is given in Fig. 4I with a graphical depiction in Fig. 8I with the frequencies when adjusting the injection pressure in Fig. 6. The characteristic lower–upper quartiles of onset times found for the investigated conditions at TDC injection timing was 180–279°CA aTDC (Fig. 5).

3.2.8. Late-cycle overspill

Prior to the subsequent TDC, fluid is occasionally observed overspilling from the orifices (Fig. 4I) with a median onset time of 352°CA. The emerging fuel appears to either be a mix of fuel and vapour, or vaporising as it emerges. However, further evidence is essential as the visual appearance of the fluid might be an illusion from the incident beam reflection. Eagle & Musculus [30] described fluid discharging from the orifices during the compression stroke, associating it with valve motion, which they referred to as 'blow-down dribble'. Although the test-bed did not incorporate valves, the peak in-cylinder gas velocity occurs near TDC may contribute to a process similar to the one they identified.

The overspill of fuel during the compression stroke occurs within a very short, specific timeframe, indicating a primary dependency on the in-cylinder conditions. The small amount of variation in onset time when varying the injection timing (Table 3) further supports this statement. However, the phenomena is not entirely independent of the injection event and resulting in-nozzle conditions, since higher injection pressures reduce the frequency of occurrence (Fig. 6). Similarly to the other phenomena discussed, the late-cycle overspill will have a strong dependence on the proportions of gas and liquid inside the nozzle after injection, which strongly depends on the injection pressure

(Section 3.2.1). If there is a large amount of fuel residing in the orifices after injection, as is the case at low IPs, then there is an abundance of fuel to partake in the overspill event.

It is thought that the process is dependent on the in-cylinder gas flow motion around the injector tip, as proposed by Eagle and Musculus [30]. It appears that this flow motion around the injector tip is present for the entire compression stroke, first inducing the in-channel fluid oscillations shortly after bottom dead centre (Section 3.2.7), then causing the fuel overspill while approaching TDC. If the flow motion influence is the sole mechanism, it suggests that the localised turbulence increases in magnitude as the cylinder volume reduces. This would be expected, since the total momentum within this flow field is not likely to reduce, it is likely to be maintained or even increased due to the piston motion [60]. Furthermore, the density of the in-cylinder gas increases, accentuating the effects of gas-fuel interactions. Compression of the medium would mean this momentum is distributed over a smaller region, increasing the effect it has on the in-nozzle liquid.

An image sequence for a typical late-cycle overspill event is given in Fig. 4I. The frequencies and timing variation when adjusting the injection angle can be found in Fig. 6 and Table 3 respectively. The characteristic lower–upper quartiles of onset times found for the investigated conditions at TDC injection timing was 351–359°CA aTDC (Fig. 5).

3.3. Phenomenological model

We present a phenomenological model to summarise our findings and proposed terminologies (Section 3.3). The fluid phenomena are included in a chronological order starting from the injection event, with particular focus on the dynamics at the orifice exits. Each event is included with its characteristic range in onset time with regards to the 1st and 3rd quartiles of the spread, (Fig. 5). The model accounts for all observed phenomena, frequent and occasional, throughout a revolution typical of low to medium load conditions with a VCO type nozzle. It should be noted that the timings and visual characteristics of the phenomena are in agreement with investigations by our institution [18,43,44] as well as others conducted independently [29,30,37,41].

4. Conclusions

High-speed microscopy was carried out on a reciprocating rapid compression machine under low (idle-like) to medium load conditions, with a DW10b instrumented valve covered orifice type injector. Focus was directed towards the transient fluid behaviour occurring on the nozzle surface and near-nozzle region between injection events. Several significant and previously unreported post-injection fluid phenomena were identified and characterised by their onset times, frequency and visible appearance. Varying the injection pressure and timing permitted assessment of the dependencies on in-nozzle and in-cylinder conditions, gaining insights into the underlying mechanisms. The phenomena and proposed terminology were summarised through a phenomenological model.

This investigation led to several findings, relevant to external deposit formation and the emission of pollutants:

- The post-injection fluid behaviour in the near nozzle region is primarily dependent on the temporal evolution of the in-cylinder conditions i.e. the gas pressure differential, and not just the instantaneous in-cylinder conditions.
- All of the post-injection phenomena observed were governed by the injection pressure due to its influence on the orifice contents after injection. A mixture of ingested gas, liquid fuel and vaporised fuel remained after the injection event and may reside until the following injection.
- Three modes of surface wetting were identified: spray wetting during the end of injection event, overspill during the expansion stroke and late-cycle overspill during the end of the compression stroke. Expansion overspill is the most frequent and is the largest contributor of nozzle wetting.
- Unburnt fuel was released into the cylinder via: large, slow moving fuel, vapour expulsion immediately after the end of injection event and droplet projection through the collapse of bubbles.
- Vapour is occasionally observed emerging from the orifices immediately after the injection event. The vapour is drawn out of the nozzle by a drop in in-cylinder pressure during the expansion stroke.

Our findings suggest that the abnormal release of fuel can be reduced through operation at higher injection pressures. The strong relationship with the temporal ICP evolution indicates high dependency with ICP differentials, considerably influenced by engine speed, engine load and the combustion event. Consequently, it appears that the detrimental effects of the observed phenomena will be more pronounced when running at low load/idling-like conditions.

These observations provide new evidence of the abnormal release of fuel throughout a diesel cycle, at the microscopic scale in a highly transient, high temperature and pressure environment. The knowledge gained enables a direct and systematic verification of numerical models for the prediction of injector wetting, hence there is a wide scope for further studies, both experimental and numerical. We suggest that future efforts should be focused on:

- Comparing these findings with a sac type nozzle. We anticipate that other phenomena, such as internal sloshing, would lead to additional fluid release events.
- Measuring the nozzle's surface temperature, so that the fluid processes can be better related to the heat transfer between nozzle and liquid films.
- Evaluating the influence of the fuel's physical properties on the fluid phenomena.

CRediT authorship contribution statement

Dan Sykes: Investigation, Methodology, Writing – original draft, Validation, Visualization. **Viacheslav Stetsyuk:** Investigation. **Jack Turner:** Investigation. **Guillaume de Sercey:** Software, Writing – review & editing. **Martin Gold:** Resources, Writing – review & editing. **Richard Pearson:** Resources. **Cyril Crua:** Conceptualization, Methodology, Resources, Writing - review & editing, Project administration, Funding acquisition, Supervision.

Declaration of competing interest

The authors declare that they have no known competing financial interests or personal relationships that could have appeared to influence the work reported in this paper.

Acknowledgements

This work was supported by the UK's Engineering and Physical Science Research Council [EPSRC grants EP/K020528/1 and iCASE Studentship 1793447] and BP International Ltd.

Appendix A. Supplementary data

Supplementary material related to this article can be found online at https://doi.org/10.1016/j.fuel.2021.122208.

References

[1] Mohammed MK, Rahman M, Bakar RA. Effects of air-fuel ratio and engine speed on performance of hydrogen fueled port injection engine. J Appl Sci 2009;9:1128–34. http://dx.doi.org/10.3923/jas.2009.1128.1134.

[2] Dec JE. A conceptual model of DI diesel combustion based on laser-sheet imaging. SAE International; 1997, http://dx.doi.org/10.4271/970873.

[3] Taskinen P. Effect of fuel spray characteristics on combustion and emission formation in a large medium speed diesel engine. SAE International; 1998, http://dx.doi.org/10.4271/982583.

[4] Zhu J, Kuti OA, Nishida K. Effects of injection pressure and ambient gas density on fuel - ambient gas mixing and combustion characteristics of D.I. diesel spray. SAE International; 2011, http://dx.doi.org/10.4271/2011-01-1819.

[5] Matsumoto S, Yamada K, Date K. Concepts and evolution of injector for common rail system. SAE International; 2012, http://dx.doi.org/10.4271/2012-01-1753.

[6] Delphi Diesel Common-Rail Systems. DFI21 injectors: heavy-duty pressure relief. 2018, URL: www.delphi.com/innovations/dfi21-injectors-heavy-duty-pressure-relief.

[7] Barker J, Richards P, Goodwin M, Wooler J. Influence of high injection pressure on diesel fuel stability: A study of resultant deposits. SAE Int J Fuels Lubr 2009;2(1):877–84. http://dx.doi.org/10.4271/2009-01-1877.

[8] Watkinson AP, Wilson DI. Chemical reaction fouling: A review. Exp Therm Fluid Sci 1997;14(4):361–74. http://dx.doi.org/10.1016/S0894-1777(96)00138-0.

[9] Tang J, Pischinger S, Lamping M, Körfer T, Tatur M, Tomazic D. Coking phenomena in nozzle orifices of Dl-diesel engines. 2009, http://dx.doi.org/10.4271/2009-01-0837.

[10] Knorsch T, Rogler P, Miller M, Wiese W. On the evaluation methods for systematic further development of direct-injection nozzles. SAE International; 2016, http://dx.doi.org/10.4271/2016-01-2200.

[11] Stępień Z. The reasons and adverse effect of internal diesel injector deposits formation. Combust Engines 2014;53(1):20–9, URL: www.combustion-engines.eu/entityfiles/files/articles_published/PTNSS-2014-103.pdf.

[12] Rounthwaite N, Mcgilvery C, Jiang J, Williams R, Giuliani F, Britton T. A chemical and morphological study of diesel injector nozzle deposits - insights into their formation and growth mechanisms. In: SAE 2017 world congress and exhibition, vol. 10. SAE International; 2017, p. 106–14. http://dx.doi.org/10.4271/2017-01-0798.

[13] Caprotti R, Bhatti N, Balfour G. Deposit control in modern diesel fuel injection systems. SAE Int J Fuels Lubr 2010;3(2):901–15. http://dx.doi.org/10.4271/2010-01-2250.

[14] Barker J, Cook S, Richards P. Sodium contamination of diesel fuel, its interaction with fuel additives and the resultant effects on filter plugging and injector fouling. SAE Int J Fuels Lubr 2013;6(3):826–38. http://dx.doi.org/10.4271/2013-01-2687.

[15] Birgel A, Ladommatos N, Aleiferis P, Milovanovic N, Lacey P, Richards P. Investigations on deposit formation in the holes of diesel injector nozzles. SAE Int J Fuels Lubr 2011;5(1):123–31. http://dx.doi.org/10.4271/2011-01-1924.

[16] Xu H, Wang C, Ma X, Sarangi AK, Weall A, Krueger-Venus J. Fuel injector deposits in direct-injection spark-ignition engines. Prog Energy Combust Sci 2015;50:63–80. http://dx.doi.org/10.1016/j.pecs.2015.02.002.

[17] Slavchov RI, Mosbach S, Kraft M, Pearson R, Filip SV. An adsorption-precipitation model for the formation of injector external deposits in internal combustion engines. Appl Energy 2018;228. http://dx.doi.org/10.1016/j.apenergy.2018.06.130.

[18] Turner JE, Stetsyuk V, Crua C, Pearson RJ, Gold MR. The effect of operating conditions on post-injection fuel discharge in an optical engine. In: 13th triennial international conference on liquid atomization and spray systems; 2015. URL https://iclass2015.tw/index.php.

[19] Leick P, Bork B, Geiler JN. Experimental characterization of tip wetting in gasoline DI injectors. In: ICLASS 2018, 14th triennial international conference on liquid atomization and spray systems; 2018. URL: www.researchgate.net/profile/Philippe_Leick/publication/326583778.

[20] Ferrari A, Mittica A, Spessa E. Benefits of hydraulic layout over driving system in piezo-injectors and proposal of a new-concept CR injector with an integrated Minirail. Appl Energy 2013;103:243–55. http://dx.doi.org/10.1016/j.apenergy.2012.09.039.

[21] Birgel A, Ladommatos N, Aleiferis P, Zülch S, Milovanovic N, Lafon V, Orlovic A, Lacey P, Richards P. Deposit formation in the holes of diesel injector nozzles: A critical review. SAE International; 2008, http://dx.doi.org/10.4271/2008-01-2383.

[22] Caprotti R, Breakspear A, Graupner O, Klaua T. Detergency requirements of future diesel injection systems. SAE International; 2005, http://dx.doi.org/10.4271/2005-01-3901.

[23] Ambrosio SD, Ferrari A. Diesel engines equipped with piezoelectric and solenoid injectors: hydraulic performance of the injectors and comparison of the emissions, noise and fuel consumption. Appl Energy 2018;211:1324–42. http://dx.doi.org/10.1016/j.apenergy.2017.11.065.

[24] Jafarmadar S. The effect of split injection on the combustion and emissions in DI and IDI diesel engines. Diesel Engine - Combust Emiss Cond Monit 2013. http://dx.doi.org/10.5772/55232.

[25] Lee C, Park S. An experimental and numerical study on fuel atomization characteristics of high-pressure diesel injection sprays. Fuel 2002;81:2417–23. http://dx.doi.org/10.1016/S0016-2361(02)00158-8.

[26] Koci CP, Ra Y, Krieger R, Andrie M, Foster DE, Siewert RM, Durrett RP. Multiple-event fuel injection investigations in a highly-dilute diesel low temperature combustion regime. SAE Int J Engines 2009;2(1):837–57. http://dx.doi.org/10.4271/2009-01-0925.

[27] Kirsch V, Reddemann MA, Palmer J, Kneer R. Zooming into primary breakup mechanisms of high-pressure automotive sprays. In: ILASS–Europe 2017, 28th conference on liquid atomization and spray systems; 2017. http://dx.doi.org/10.4995/ILASS2017.2017.4603.

[28] Fitzgerald RP, Bazyn T. Dribble quantification for diesel fuel injectors. In: ICLASS 2018, 14th triennial international conference on liquid atomization and spray systems; 2018. URL: www.iclass2018.org/program/s204.html.

[29] Pos R. Spatio-temporal evolution of diesel sprays using high-speed optical diagnostics. [Thesis], 2016, URL: http://bura.brunel.ac.uk/handle/2438/14481.

[30] Eagle W, Musculus M. Cinema-stereo imaging of fuel dribble after the end of injection in an optical heavy-duty diesel engine. In: Thiesel conference proceedings; 2014.

[31] Moon S, Huang W, Li Z, Wang J. End-of-injection fuel dribble of multi-hole diesel injector: Comprehensive investigation of phenomenon and discussion on control strategy. Appl Energy 2016;179:7–16. http://dx.doi.org/10.1016/j.apenergy.2016.06.116.

[32] Papadopoulos N, Aleiferis P. Numerical modelling of the in-nozzle flow of a diesel injector with moving needle during and after the end of a full injection event. SAE Int J Engines 2015;8(5):2285–302. http://dx.doi.org/10.4271/2015-24-2472.

[33] Kotnik G, Tibaut P, Krankenedl W, Morozov A. A simulation methodology to lower GDI soot emissions by reducing nozzle tip wetting. In: Liebl J, editor. Simulation und test 2018. Springer Fachmedien Wiesbaden; 2019, p. 225–37. http://dx.doi.org/10.1007/978-3-658-25294-6.

[34] Battistoni M, Xue Q, Som S. Large-eddy simulation (LES) of transient spray: Start and end of injection phenomena. IFP Energies Nouvelles International Conference 2016;71(1). http://dx.doi.org/10.2516/ogst/2015024.

[35] Sechenyh V, Duke DJ, Swantek AB, Matusik KE, Kastengren AL, Powell CF, Viera A, Payri R, Crua C. Quantitative analysis of dribble volumes and rates using three-dimensional reconstruction of X-ray and diffused back-illumination images of diesel sprays. Int J Engine Res 2019;21(1):43–54. http://dx.doi.org/10.1177/1468087419860955.

[36] Duke DJ, Kastengren A, Swantek AB, Sovis N, Fezzaa K, Neroorkar K, Moulai M, Powell CF, Schmidt DP. Comparing simulations and X-ray measurements of a cavitating nozzle. In: ILASS-Americas 26th annual conference on liquid atomization and spray systems; 2014. http://dx.doi.org/10.1615/AtomizSpr.2013008340.

[37] Moon S, Komada K, Li Z, Wang J, Kimijima T, Arima T, Maeda Y. High-speed X-ray imaging of in-nozzle cavitation and emerging jet flow of multi-hole GDI injector under practical operating conditions. In: ICLASS 2015, 13th Triennial International Conference on Liquid Atomization and Spray Systems; 2015. URL: www.researchgate.net/publication/285720857.

[38] Chouak M, Mousseau A, Reveillon D, Dufresne L, Seers P. Study of transient effects in the internal flow of a diesel fuel injector. SAE International; 2015, http://dx.doi.org/10.4271/2015-01-0923.

[39] Hirt CW, Nichols BD. Volume of fluid (VOF) method for the dynamics of free boundaries. J Comput Phys 1981;39(1):201–25. http://dx.doi.org/10.1016/0021-9991(81)90145-5.

[40] Battistoni M, Poggiani C, Som S. Prediction of the nozzle flow and jet characteristics at start and end of injection: Transient behaviors. 2015, http://dx.doi.org/10.4271/2015-01-1850.

[41] Swantek AB, Duke D, Tilocco FZ, Sovis N, Powell CF, Kastengren AL. End of injection, mass expulsion behaviors in single hole diesel fuel injectors. In: Proceedings of ILASS Americas; 2014. URL: http://www.ilass.org/2/database/Detail.aspx?AbstractID=906.

[42] Manin J, Pickett LM, Yasutomi K. Stereoscopic high-speed microscopy to understand transient internal flow processes in high-pressure nozzles. Exp Therm Fluid Sci 2020;114:110027. http://dx.doi.org/10.1016/j.expthermflusci.2019.110027.

[43] Sykes D, Sercey GD, Gold M, Pearson R, Crua C. Visual analyses of end of injection liquid structures and the behaviour of nozzle surface-bound fuel in a direct injection diesel engine. SAE International; 2019, http://dx.doi.org/10.4271/2019-01-0059.

[44] Sykes D, Turner J, Stetsyuk V, Sercey GD, Gold M, Pearson R, Crua C. Quantitative characterisations of spray deposited liquid films and post-injection discharge on diesel injectors. Fuel 2021;289. http://dx.doi.org/10.1016/j.fuel.2020.119833.

[45] Cyril C. Combustion processes in a Diesel engine. [Thesis], 2002, URL: http://eprints.brighton.ac.uk/id/eprint/1161.

[46] Gander A, Sykes D, Payri R, de Sercey G, Kennaird D, Gold M, Pearson RJ, Crua C. High-speed infrared measurement of injector tip temperature during diesel engine operation. Energies 2021;14(15):4584. http://dx.doi.org/10.3390/en14154584.

[47] Musculus MB, Miles PC, Pickett LM. Conceptual models for partially premixed low-temperature diesel combustion. Prog Energy Combust Sci 2013;39(2):246–83. http://dx.doi.org/10.1016/j.pecs.2012.09.001.

[48] Payri R, Salvador FJ, Gimeno J, Morena JDL. Macroscopic behavior of diesel sprays in the near-nozzle field. SAE Int J Engines 2008;1(1):528–36. http://dx.doi.org/10.4271/2008-01-0929.
[49] Crua C, Heikal MR, Gold MR. Microscopic imaging of the initial stage of diesel spray formation. Fuel 2015;157(Supplement C):140–50. http://dx.doi.org/10.1016/j.fuel.2015.04.041.
[50] Yasutomi K, Hwang J, Pickett LM, Sforzo B, Matusik K, Powell CF. Transient internal nozzle flow in transparent multi-hole diesel injector. SAE International; 2020, http://dx.doi.org/10.4271/2020-01-0830.
[51] Wang Z, Li Y, Wang C, Xu H, Wyszynski ML. Experimental study on primary breakup of diesel spray under cold start conditions. Fuel 2016;183:617–26. http://dx.doi.org/10.1016/j.fuel.2016.06.067.
[52] Abers PM, Cenker E, Yasutomi K, Hwang J, Pickett LM. Effect of pressure cycling on gas exchange in a transparent fuel injector. SAE International; 2019, http://dx.doi.org/10.4271/2019-01-2280.
[53] Tonini S, Gavaises M, Theodorakakos A. The role of droplet fragmentation in high-pressure evaporating diesel sprays. Int J Therm Sci 2009;48(3):554–72. http://dx.doi.org/10.1016/j.ijthermalsci.2008.03.020.
[54] Lemmon EW, Huber ML. Thermodynamic properties of n-dodecane. Energy Fuels 2004;18(4):960–7. http://dx.doi.org/10.1021/ef0341062.
[55] Lockett R, Jeshani M, Makri K, Price R. An optical characterization of atomization in non-evaporating diesel sprays. SAE International; 2016, http://dx.doi.org/10.4271/2016-01-0865.
[56] Westlye FR, Battistoni M, Skeen SA, Manin J, Pickett LM, Ivarsson A. Penetration and combustion characterization of cavitating and non-cavitating fuel injectors under diesel engine conditions. SAE International; 2016, http://dx.doi.org/10.4271/2016-01-0860.
[57] Brennen C. Cavitation and bubble dynamics, vol. 44. 1995, http://dx.doi.org/10.1017/CBO9781107338760.
[58] Henry W. Experiments on the quantity of gases absorbed by water, at different temperatures, and under different pressures. Philos Trans R Soc 1803;93:29–76. http://dx.doi.org/10.1098/rstl.1803.0004.
[59] Rupprecht SD, Faeth GM. Investigation of air solubility in jet a fuel at high pressures. Report, The Pennsylvania State University; 1981, URL https://ntrs.nasa.gov/citations/19810012682.
[60] Rota C, Morgan R, Osborne R, Mason D, Heikal M, Matrisciano A, Mustafa K. A process for an efficient heat release prediction at multiple engine speeds and valve timings in the early stage of gasoline engine development. SAE International; 2019, http://dx.doi.org/10.4271/2019-24-0085.